Application of percolation theory to microtomography of structured media: Percolation threshold, critical exponents, and upscaling

Jie Liu[1,2,3] and Klaus Regenauer-Lieb[1,2,3,4]

[1]*Computational Geoscience, CSIRO Earth Science and Resource Engineering, P. O. Box 1130, Bentley, Western Australia 6102, Australia*

[2]*School of Earth and Environment, University of Western Australia, 35 Stirling Highway, Western Australia 6009, Australia*

[3]*Multi-scale Earth System Dynamics, University of Western Australia, 35 Stirling Highway, Western Australia 6009, Australia*

[4]*Western Australian Geothermal Center of Excellence, P. O. Box 1130, Bentley, Western Australia 6102, Australia*

(Received 15 June 2010; revised manuscript received 25 September 2010; published 18 January 2011)

Percolation theory provides a tool for linking microstructure and macroscopic material properties. In this paper, percolation theory is applied to the analysis of microtomographic images for the purpose of deriving scaling laws for upscaling of properties. We have tested the acquisition of quantities such as percolation threshold, crossover length, fractal dimension, and critical exponent of correlation length from microtomography. By inflating or deflating the target phase and percolation analysis, we can get a critical model and an estimation of the percolation threshold. The crossover length is determined from the critical model by numerical simulation. The fractal dimension can be obtained either from the critical model or from the relative size distribution of clusters. Local probabilities of percolation are used to extract the critical exponent of the correlation length. For near-isotropic samples such as sandstone and bread, the approach works very well. For strongly anisotropic samples, such as highly deformed rock (mylonite) and a tree branch, the percolation threshold and fractal dimension can be assessed with accuracy. However, the uncertainty of the correlation length makes it difficult to accurately extract its critical exponents. Therefore, this aspect of percolation theory cannot be reliably used for upscaling properties of strongly anisotropic media. Other methods of upscaling have to be used for such media.

DOI: 10.1103/PhysRevE.83.016106 PACS number(s): 89.75.Da, 89.75.Fb, 89.90.+n, 05.10.−a

I. INTRODUCTION

Micro computed tomography (micro-CT) or microtomography is becoming an important technique for research of material properties [1]. We evaluate here the use of percolation theory as a valuable tool for upscaling from the microtomography scale to the macroscale. Upscaling is a widely used method in computational hydrodynamics and mechanics for solving the problem of a statistical distribution of transport or mechanical coefficients (or properties) on a small scale, and linking these to the statistics of such transport or mechanical values on a larger scale [2]. Upscaling can be understood as the equivalent concept of a scaling function, with the aim of derivation of the renormalization constant normalized to that at a given reference scale. Renormalization-group-invariant properties have a much wider applicability in condensed matter and high-energy physics, while the applied material sciences and geophysical applications are often more focused on very restrictive applications. This paper presents examples of upscaling in applied material sciences. The fundamental analysis can be expanded to both research fields.

Percolation theory focuses on the connectivity of sites (or bonds) of different models, critical phenomena, and relevant quantities [3] (basic concepts of percolation theory are summarized in Appendix A). From percolation theory, critical exponents extracted from critical phenomena are related to scaling laws, and scaling laws enable upscaling or downscaling of the characteristics recognized at a certain scale. Mathematically, percolation theory deals with random networks and it can be applied to most fields of natural science. As percolation research is mostly based on random models, the objects being studied are stochastic geometries that are numerically or experimentally created in a forward way. The application of percolation theory to finite-size scaling derived from microtomography analyses of a CT scan has only been investigated in pilot studies for particular materials [4]. For this reason, percolation theory, albeit being recognized as a powerful tool to explore general laws of materials in nature, has not yet gained wide acceptance in the analysis of direct observational data such as those obtained from microtomography. In this paper we test and evaluate the use of percolation theory in a wide range of internally structured media.

Microtomography provides three-dimensional (3D) microscale images via nondestructive scanning. 3D images showing the internal structure of objects lead to the possibility of the study of the spatial distribution and evolution of phases or material-components at the micro- and nanoscale. It is becoming one of the most important frontier technologies applied in medical, biomedical, and material sciences. Stock [5] gives an excellent review of the applications of microtomography to material science. Owing to the finite size of the image sampling chip (e.g., 2048×2048 pixels normally), the limitation of microtomography lies in the relationship of the length scale and resolution of the images or samples: the higher the resolution, the smaller is the length scale that can be imaged in a single scan. This leads to the immediate challenge of detecting the microstructure of the material in finer and finer resolution and then of connecting it to the macroscale where conventional continuum mechanics applies. Scaling laws of percolation theory provide an opportunity to connect the microscale to the macroscale.

Previous applications of percolation theory to micro-CT analysis are sparse, especially the explicit derivation of quantities for percolation. Ikeda *et al.* [6] investigated the 3D interconnection, shape, and correlation function of a

granite sample. Nakashima and Kamiya [7] developed a program for the analysis of pore connectivity and anisotropic tortuosity of porous rocks. In the study of Navarre-Sitchler *et al.* [8], micro-CT data were used to construct a numerical pore network model. Using percolation theory, these authors determined the upscaled effective diffusivities as a function of total porosity, and also determined the percolation threshold by experiments. Liu *et al.* [9] presented an improved estimation of percolation and anisotropic permeability from 3D x-ray microtomography using stochastic analyses. Recently, Pringle *et al.* [4] analyzed the percolation threshold of the brine microstructure of sea ice using the finite-size-scaling scheme of percolation theory from a series of samples at different temperatures. Although percolation theory has thus proven to be a useful tool for analysis of microtomography, open questions remain.

The first question is how to derive the percolation threshold from static natural data. It is the most important question because the percolation threshold is of great significance to material properties. Generally, the percolation threshold is determined by creating a series of models numerically or experimentally. These models are random or for some assumed structure. However, the percolation thresholds calculated from random or assumed models [3,10], are not suitable for other models with a given structure as obtained, for instance, from a CT scan of natural samples. Pringle and co-authors [4] presented the first successful detection of the percolation threshold from images of natural samples. The crucial prerequisite for this achievement was the availability of a series of samples of sea ice with different porosities at different temperatures. However, for most natural samples, it is very difficult to derive the percolation threshold, because of the unavailability of a series of models with different volume fractions of the specific structure. We will contribute to this point as described in the methodology section and Appendix B.

The second question is whether or not we can derive critical exponents and fractal dimension from scans of natural samples. Critical exponents and fractal dimensions are recognized as universally invariant and can be used for upscaling or downscaling of models and properties. Most universally invariant quantities have been determined theoretically for different lattices [3]. These quantities are expected to change in a range around the theoretical values for specific problems. It is therefore important to compare the predicted theoretical values with those obtained from natural samples. This comparison is a prerequisite for robust upscaling of the characteristics of individual microtomography. To the best of our knowledge, no critical exponents extracted from microtomographic images have yet been reported in the publicly available literature. In this study we will present an analysis of the extraction of exponents.

A number of methods for upscaling have been developed, using percolation theory, effective-medium theory, and stochastic homogenization, among other methods [11]. We propose that whenever possible percolation theory should be used for upscaling of microtomography as the first choice since it is the most direct method based on the observed statistics. The elaboration of this method is the main subject of the paper.

II. METHODS

This study is based on our previous research [9] into stochastic analysis of microstructure and the determination of a representative volume element (RVE). The probabilities of porosity, percolation, and anisotropy are calculated by using the moving window method. Then, by adopting the idea of finite-size scaling, the size of the RVE is determined when these probabilities are convergent with the increase of the sub-volume-size L of the moving window. A RVE is a statistically representative volume containing a sufficiently large set of microstructure elements such that their influence on the average macroscopic property (porosity, elasticity, permeability, etc.) has converged when a larger volume element is taken.

A RVE is insufficient for upscaling because the extrapolation from microscale to macroscale is also controlled by some percolation quantities. For a complex multiscale system, it is necessary to extract universally invariant quantities and basic percolation quantities to ensure the upscaling for specific structures. In the following we present the main quantities of percolation theory that are connected to scaling laws, the method of extracting these quantities, and the relationships of these quantities within a multiscale strategy based on microtomographic data.

A. Percolation and scaling quantities from microtomography

The original data of microtomography are 8–32 bit images from x-ray CT scans. Preprocessing is necessary to select and label the phase of interest. This target phase can be pores, grains, or any kind of material that is separated from the matrix by its intensity value in the images. The intensity corresponds to the atomic number of the material, a high atomic number giving a bright image and a low atomic number giving a darker image. The bitmap images are converted into binary images through a segmentation process that relies on attributing an intensity spectrum to the target phase. This segmentation is used to construct a 3D binary model from the tomography slices. The binary microstructural model could be considered as a simple cubic lattice model, in which every cubic cell (or site) is equivalent to a voxel in image processing. In the simple cubic lattice model, the nearest neighbors are voxels with one common plane. A cluster is a group of nearest neighbors of the same material which are connected to each other. The labeling of clusters is a process of giving all cells within the same cluster the same label. The Hoshen-Kopelman algorithm [12] is used to reduce the computing time in this procedure.

1. Percolation threshold

The percolation threshold p_c is defined as the lowest volume fraction at which a percolating cluster begins to form. To find the percolation threshold, it is essential to have models with similar structures but different volume fractions.

We introduce here a morphological technique to determine the percolation threshold of a microstructure by deflating (shrinking) and inflating (expanding) the target phase (see Appendix B). A deflation operation consists in moving the boundaries of clusters one voxel inward in all directions (positive and negative, in the x, y, and z directions). It reduces the volume fraction and breaks the weakest bond. An inflation

operation consists in moving boundaries outward. It increases the volume fraction and might cause the nearest clusters to be connected. Both operations keep the orientation of clusters. In this way, a series of derivative models is created from the original model. These models have different volume fractions but retain a structure similar to that of the original sample. By analyzing the percolation of these models, the critical model is identified as the percolating model that is the closest to nonpercolating models. The volume fraction of the critical model is recognized as the percolation threshold. The detailed algorithm for deflating and inflating and its features are given in Appendix B.

This method is suitable to any kind of structure. However, two limitations need to be considered: (1) By shrinking and expanding the target phase, we can estimate the percolation threshold, but we cannot give an accurate value, because these operations cannot create continuous volume fractions. Moving boundaries in positive and negative directions in separate operations and creating intermediate (half-step) deflated or inflated models can improve the accuracy of the algorithm. (2) Deflation and inflation represent one simple way of changing the volume fraction of the microstructure. It is ideal for isotropic clusters. For anisotropic clusters, although deflation and inflation do not change the orientation of individual clusters, they gradually change the ratio of the principal axes of the orientation tensors. In our future work, we will present methods particularly suited for anisotropic cases because they preserve the ratio of the principal axes of tensors in the deflation and inflation operations. The rationale of this paper is to first benchmark the simpler method.

2. Critical exponents

There are several different critical exponents, such as the critical exponent of the correlation length, critical exponents of the mean cluster size, the critical exponent of strength, the Fisher exponent, the specific heat exponent, etc., but only two are independent. In most cases the critical exponent of the correlation length is the easiest to calculate.

The correlation length ξ represents some average distance between any two sites belonging to the same cluster [3]. It is defined as

$$\xi^2 = \frac{2\sum_s R_s^2 s^2 n_s}{\sum_s s^2 n_s}, \tag{1}$$

where s is the number of sites of a cluster, n_s is the number of such s-site clusters per lattice site, and R_s defined as

$$R_s^2 = \sum_{i=1}^{s} (|x_i - x_0|^2/s) \tag{2}$$

is the radius of a complex cluster of s sites; here $x_0 = \sum_{i=1}^{s} (x_i/s)$ is the position of the center of mass of the cluster, and x_i is the position of the ith site in the cluster. The correlation length ξ diverges when the volume fraction p approaches the percolation threshold p_c as

$$\xi \propto |p - p_c|^{-\nu}. \tag{3}$$

Here ν is the critical exponent of the correlation length (or correlation length exponent). It can be extracted by a finite-size-scaling scheme from the local percolation probabilities $\lambda(p, L)$ of different subvolume sizes L and different volume fractions p [9,13]. The finite-size-scaling scheme has the relationship

$$p_{\text{av}} - p_c \propto L^{-1/\nu}, \tag{4}$$

where $p_{\text{av}} = \int p\,(d\lambda/dp)\,dp$, and p_c is the volume fraction when a nonzero probability of percolation is first detected for the corresponding subvolume size L. Thus, with a group of results of local percolation probabilities, the critical exponent of the correlation length ν can be obtained by fitting $\log_{10} L$ to $\log_{10}(p_{\text{av}} - p_c)$.

3. Fractal dimension

The fractal dimension D is the most popular measure for scale invariance currently used in the literature. It is derived from a power law describing a characteristic versus a statistical variable. In percolation theory, the fractal dimension is one of the variables in scaling laws together with other critical exponents. The fractal dimension can be found from the relative size and the number of clusters defined as

$$D = \frac{\log_{10} N\left(l \geqslant \frac{R}{R_{\max}}\right)}{\log_{10} l\left(= \frac{R}{R_{\max}}\right)}, \tag{5}$$

where the relative size of cluster l is the radius in Eq. (2) normalized by the radius of the largest cluster; the number of clusters N includes clusters that are equal to or larger than the normalized relative radius.

B. Multiscale strategy

We evaluate the usefulness of extraction of percolation quantities as one method of upscaling material properties from microtomography. From percolation theory, the relationships of critical exponents, including the fractal dimension D and lattice dimension d, are scaling laws [3]. They have the form of $D = d - \beta/\nu$, $\nu D = \beta + \gamma$, $2 - \alpha = 2\beta + \gamma$, etc., where β is the critical exponent of strength, γ is the critical exponent of mean cluster size, and α is the specific heat exponent. For the 3D simple cubic lattice model, we have the lattice dimension of $d = 3$. Since there are only two independent critical exponents, the fractal dimension can be one of these; with any two critical exponents we can derive all other critical exponents. These critical exponents and scaling laws are used for upscaling of properties. The percolation threshold and correlation length are also basic quantities considered in upscaling. The main idea is illustrated in Fig. 1.

The stochastic analysis (left column of Fig. 1) was described in our previous research [9]; it provides the probabilities of porosity, percolation, and anisotropy of different scales (limited to the 3D microstructure model), and can be used to determine the size of the RVE. Different numerical simulation methods, such as finite-element, finite-difference, and lattice-Boltzmann methods, have been used to compute material properties of microstructures [14]. Previous computations were based on arbitrarily selected volume size. We suggest that simulations should be based on the RVE, since only the RVE can represent the general characteristics.

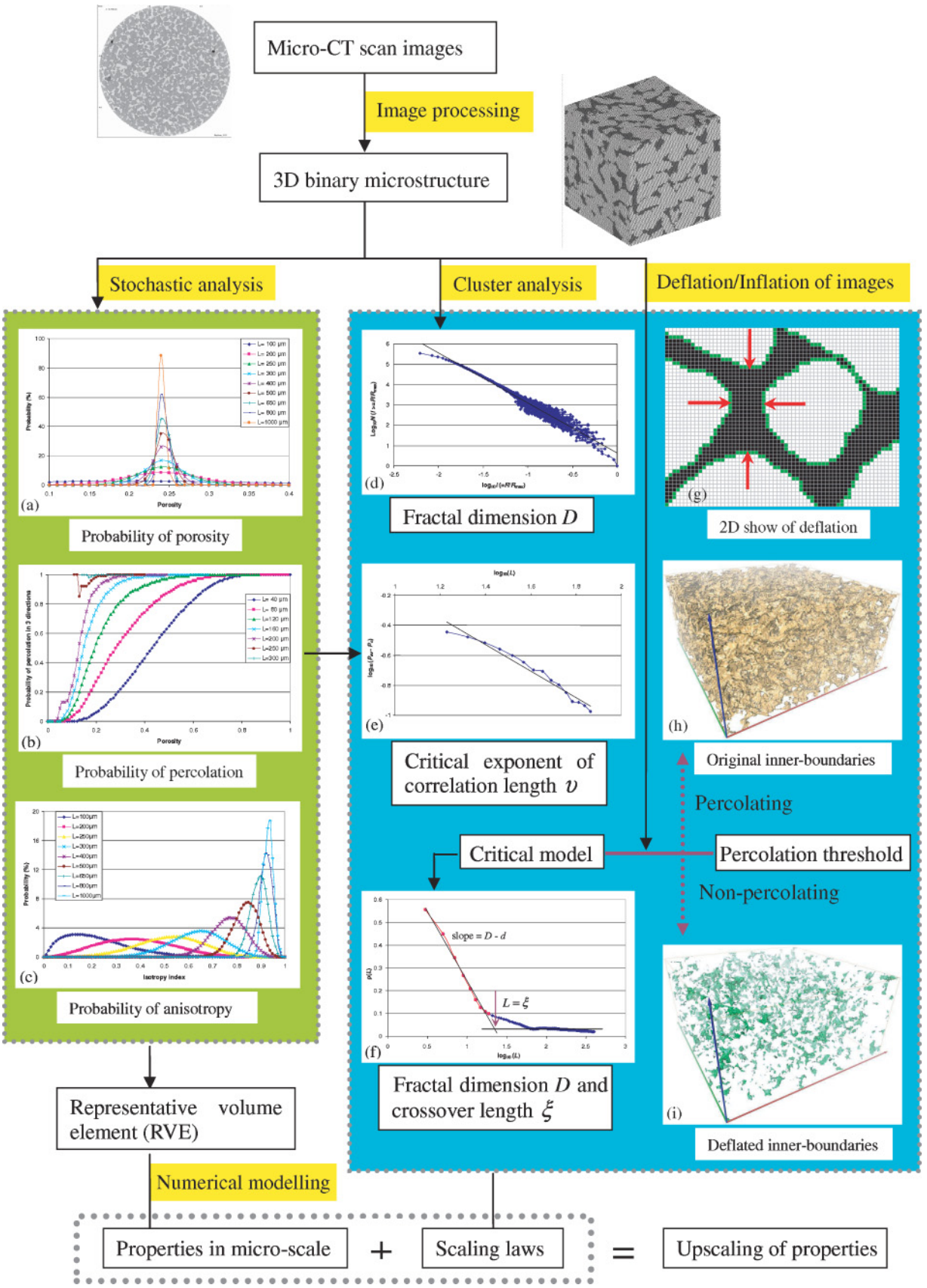

FIG. 1. (Color online) Strategy from microtomography to macroscale properties.

The right side of Fig. 1 describes the method used in this paper: (1) cluster analysis for deriving the fractal dimension D; (2) finite-size-scaling scheme using the probability of percolation to derive the critical exponent of the correlation length ν; (3) inflation or deflation of the original structure to determine the percolation threshold from a series of derivative models. The critical model with percolation threshold provides another way to extract the fractal dimension D and the crossover length ξ. The crossover length is a special correlation length separating the critical and noncritical behavior. When we get the critical exponent of the correlation length ν and the fractal dimension D from individual samples, the final derived scaling laws are exact for the specific structures.

III. CASE STUDIES

We present five samples to show the capability of our approach for different structured two-phase media. The samples are a synthetic sandstone sample, a bread sample, two highly deformed rock samples, and one tree branch. Only the pore structures are analyzed in these samples; thus the volume fraction used above is replaced by the porosity in the following analyses.

A. Synthetic sandstone sample as a benchmark

The synthetic sandstone sample is made by compacting glass beads and cementing with a calcite *in situ* precipitation system. The porosity of the sample is 24.44%. It is percolating in all three directions and almost isotropic. More detailed information about the sample can be found in [9]. The RVE size of the sandstone sample was defined as 1 mm^3. Hence we analyze a cube of 1 mm^3 which corresponds to a 400^3-voxel model.

Porosities and percolation results are listed in Table I for original and derivative models obtained by deflating and inflating the pore structure of the samples. From the second and third columns, we can see that the sixth deflated derivative model of the sandstone sample with a porosity of 3.94% is percolating only in the z direction. Models with more deflation steps are not percolating. Models with fewer deflation steps are percolating in three directions. We recognize the sixth deflated model as the critical model because it is the percolating model which is the closest to the nonpercolating models. The associated porosity of 3.94% is recognized as the percolation threshold.

The value of the percolation threshold obtained by our method for the synthetic sandstone is an order of magnitude smaller than that expected for the simple cubic lattice model obtained from random number simulations (31.16%) [3]. The pores of the synthetic sandstone are unlike the mathematical random lattice model as they are not randomly distributed in 3D space, but structured. This structure derives from the compaction mechanism and the close packing of grains, which are not considered in the random number models. This compaction can be simulated mathematically. Bentz [15] created virtual permeable discrete microstructural models and obtained a similar percolation threshold of $(3.2 \pm 0.4)\%$ for porous media. This result is similar to our value of 3.94% and strongly supports the result for the percolation threshold obtained from our synthetic sandstone sample.

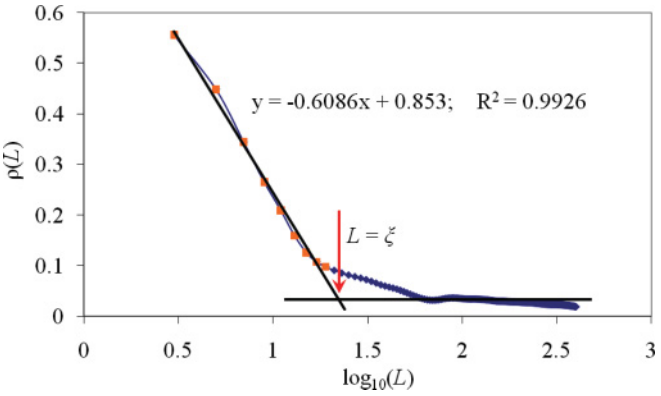

FIG. 2. (Color online) Mass density $\rho(L)$ versus cubic size L of the derivative critical model of the sandstone sample. The slope for small cubic size L corresponds to $D - d$; thus the fractal dimension D is obtained. The plateau corresponds to the porosity for large cubic size L. The transition between the sloping line and the plateau corresponds to the crossover length ξ.

We can extract more information from the critical model following the statistics of the 2D simulation proposed by Kapitulnik *et al.* [16]. The analyzed variable is the mass density $\rho(L)$, which is the number of voxels belonging to the largest cluster per lattice in the measured cube with side length L. When the porosity $\phi > p_c$, $\rho(L) = \text{const}$; while at the percolation threshold, the relationship has the form of $\rho(L) \propto L^{D-d}$. As shown in Fig. 2, $\rho(L)$ is linearly decreasing with $\log_{10}(L)$ when $L$is small. The fitting slope is $D - d$ and equal to -0.609; thus the fractal dimension $D = 2.391$ is obtained, which is close to the theoretical result 2.5 [3]. For increasing side length the mass density converges to a constant value. The transition from sloping line to plateau should correspond to the crossover length ξ separating the critical from the noncritical behavior. In Fig. 2 the transition occurs at $\log_{10}(L) = 1.3$; thus ξ is around 20 voxels, corresponding to 50 μm.

Figure 2 gives a typical illustration of a scale transition showing that extrapolation from the microscale to the macroscale is controlled by percolation quantities. An upscaling of permeabilities obtained in a laboratory test to a large field scale cannot be done without considering percolation quantities. Assume, for instance, that a laboratory measurement of porosity in a 1 mm^3 sandstone sample from a reservoir is used in conjunction with classical permeability-porosity relationships to derive the productivity of a large-scale oil field. The sample is assumed to have reached the percolation threshold but it is smaller than the correlation length. Since $\rho(L) \propto L^{D-d}$ it follows that for a theoretical fractal dimension of $D = 2.5$ and a corresponding $d = 3$, the ratio of $\rho(L = 10^6)$ to $\rho(L = 1)$ for the two scales of $L = 1$ km and $L = 1$ mm is 1/1000. This implies that the amount of extractable oil from the reservoir of a scale of 1 km is only 1/1000 of that predicted by 1 mm^3 sample with $\rho(L) = \text{const}$. Stauffer and Aharony [3] gave this example to emphasize the necessity for deriving additional scaling parameters for the prediction of oil recovery in a petroleum reservoir.

We proceed now to a comparison with a measured percolation parameter from the synthetic sandstone. Before upscaling

material properties we need to identify the other critical exponents. From the stochastic analysis [9], a series of local probabilities of percolation in three directions of the sandstone sample is obtained for subvolume size from 17 to 73 voxels; see Fig. 3(a). With these probabilities and fitting $\log_{10} L$ and $\log_{10}(p_{av} - p_c)$, the critical exponent of the correlation length $\nu = 0.885$ is obtained [Fig. 3(b)] for our synthetic sandstone sample. It is very close to the theoretical analysis result of 0.88 [3]. In addition, the percolation thresholds of finite sizes in Fig. 3(a) converge from 7% to 3%, asymptotically.

The analysis showed that the correlation length exponent and the fractal dimension extracted from the sandstone sample are close to the theoretical values. The percolation threshold of this structured medium is 3.94%, while the sample has a porosity of 24.4%, which is far above the percolation threshold. In addition, the crossover length of the critical model is relatively small, i.e., 50 μm. From Eq. (3) we derive that the higher the porosity the smaller is the correlation length; therefore the crossover length of the original synthetic sandstone sample should be smaller than 50 μm. Based upon these observations, we can directly use the transport properties obtained from the microscale for upscale modeling to the macroscale. This deduction is verified up to laboratory scale; see Appendix C. The adjustment performed in the example given by Stauffer and Aharony [3] does not apply in this sample. This statement is only true when the sample is proven to be above the crossover length and the percolation threshold.

B. Bread sample representing high-porosity media

Fermented bakery products such as bread and cake are characterized by a high porosity. Previous x-ray CT scan analyses on the microstructure of bread aimed at deriving mechanical properties [17]. Here, we present an analysis of the percolation threshold and critical exponents. The resolution of the bread sample in our case study is 18.33 μm and the porosity is 82%. The pore structure of the bread sample is comparable to the grain structure of the sandstone sample. The percolation threshold is 24.5% as obtained from the deflation of the cells; see Table I. This percolation threshold is the highest of all investigated samples, and it is close to the result of 3D random models of 33.6%. The probabilities of percolation and the finite-size-scaling scheme resolve a critical exponent of the correlation length of 0.906, which is slightly larger than the theoretical value of 0.88 [3]. This result is limited by the relatively large size of the pores compared to the size of the subvolume. For $L \geqslant 20$ voxels, no complete curves can be created for local probabilities of percolation because of the high porosity of the breads. The range of L is therefore extremely limited in finite-size scaling. Thus, the result of the analysis, although meaningful, suffers from lower reliability. The fractal dimension from the mass density versus L is 2.3 and the crossover length is around 24 voxels. This case study gives reasonable results and confirms that the approach is suitable for high-porosity samples with some stipulations on reliability.

C. Complex structure of a highly deformed rock

Fusseis *et al.* [18] analyzed highly deformed rocks (mylonites) from the Redbank Shear Zone in central Australia. The investigated sample shows a complex, highly anisotropic arrangement of micropores which are related to the shear deformation. Liu *et al.* [19] applied the stochastic method to two subsamples from the perimeter and the center of the shear zone, respectively. In the following discussion, we focus on the applicability of the analysis presented above and refer to the cited literature for a micromechanical and fluid flow interpretation of the results. We discuss results for a cube of 901^3 voxels from the 2048^3 image volume for both subsamples with the resolution of 1.6 μm.

The porosity and percolation of the original and deflated and inflated models are listed in Table I. For the subsample from the perimeter of the shear zone, the second inflation step with porosity 6.71% delivers the first percolation in three orthogonal directions. The original and deflated models and the first inflation step are not percolating in any direction. For the subsample from the center of the shear zone, all deflated models are not percolating; the original model with

TABLE I. Porosity and percolation of sampling models. In the operation column, 0 denotes the original model, negative values represent deflating, and positive values represent inflating. Critical models and percolation threshold are set in bold.

Operation	Sandstone		Bread		Mylonite–perimeter		Mylonite–center		Tree branch	
	ϕ (%)	Perc	ϕ (%)	Perc	ϕ (%)	Perc	ϕ (%)	Perc	ϕ (%)	Perc
−11			21.46	0						
−10			**24.48**	***y***						
−9			27.90	3						
−8	1.33	0	31.76	3						
−7	2.38	0	36.12	3						
−6	**3.94**	***z***	41.00	3						
−5	6.09	3	46.44	3						
−4	8.82	3	52.47	3					0.06	0
−3	12.10	3	59.11	3			0.0009	0	**0.31**	***z***
−2	15.84	3	66.35	3	0.0023	0	0.016	0	1.20	*z*
−1	19.96	3	74.13	3	0.102	0	0.206	0	3.88	*z*
0	24.42	3	82.16	3	1.090	0	**2.704**	**3**	11.99	*z*
+1					3.27	0	8.45	3		
+2					**6.71**	**3**	17.25	3		
+3					11.11	3	27.61	3		

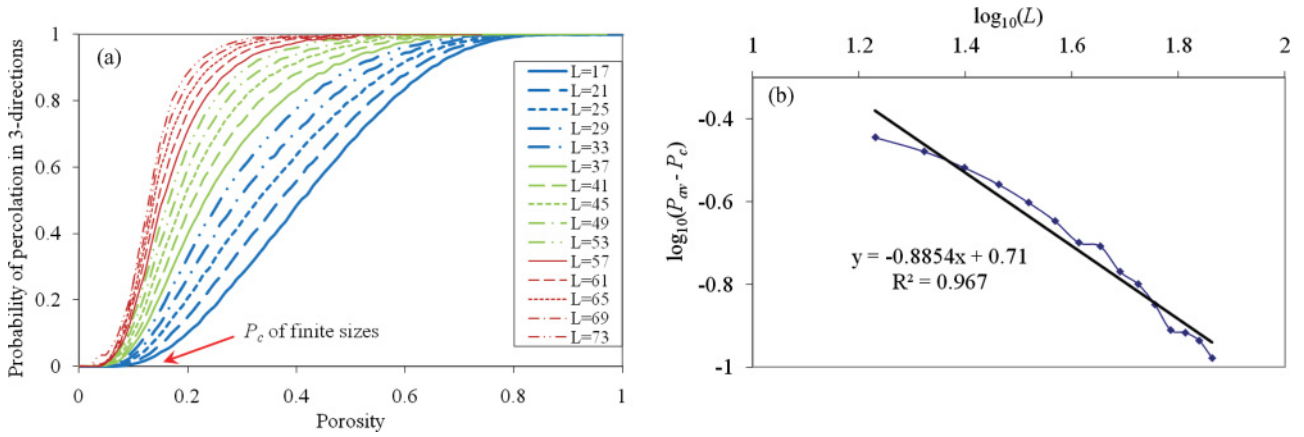

FIG. 3. (Color online) Sandstone sample: (a) local probabilities of percolation $\lambda(p,L)$, the starting points of $\lambda(p,L) \neq 0$ representing the percolation threshold of finite sizes range from 0.03 to 0.07; and (b) the fitting of the correlation length exponent based on the results of (a) and the finite-size-scaling scheme of Eq. (4).

a porosity of 2.704% is percolating, and all inflated models are percolating as well. Thus the percolation threshold for the perimeter subsample is 6.71%, and for the shear zone center sub-sample is 2.704%. The pore structure in the perimeter subsample is irregular; and the center subsample has two perpendicular fractures [19]. For such a fractured model a low percolation threshold seems reasonable.

Figure 4 gives the relationships of cluster size and cluster number for the perimeter subsample. In the double-logarithm coordinates [Fig. 4(a)], the cluster number decreases almost linearly with increase in the cluster size for small cluster sizes. There is a transition segment of "medium-size clusters" which generally have 2–10 clusters of the same size. Large-size clusters are often unique. The linear relationship between the logarithms of the cluster size and cluster number does not define a fractal dimension. The fractal dimension can be found instead from the relative cluster size with respect to radius and the number of clusters defined in Eq. (5). The fractal dimension is 2.457 for the perimeter subsample, as shown in Fig. 4(b). For the shear zone center subsample (not pictured), it is 2.825.

The stochastic analysis showed that the perimeter subsample is not percolating at a scale larger than 400 μm [19]. From the local probabilities of percolation of different subvolume sizes, we obtained a critical exponent of the correlation length of 0.726. This value is much less than that of the sandstone sample and the theoretical result. For the center subsample, the pore structure is extremely anisotropic. It has a low probability of percolation for small subvolume sizes, but it is percolating when $L \geqslant 400$ μm [19]. The local probabilities of percolation for different L are not regular as shown in Fig. 3(a), and it is difficult to fit a critical exponent.

D. Strongly anisotropic tree branch sample

Our tree branch sample is an *Acacia ayersiana* with diameter of 6.8 mm. The branch is scanned with a resolution of 3.4 μm for each voxel. Stochastic analysis shows that the probabilities of porosity, percolation, and anisotropy are convergent when the subvolume size is 300 voxels for the central part of the sample. We analyze the slightly larger volume of a 400-voxel cube using the same methodology.

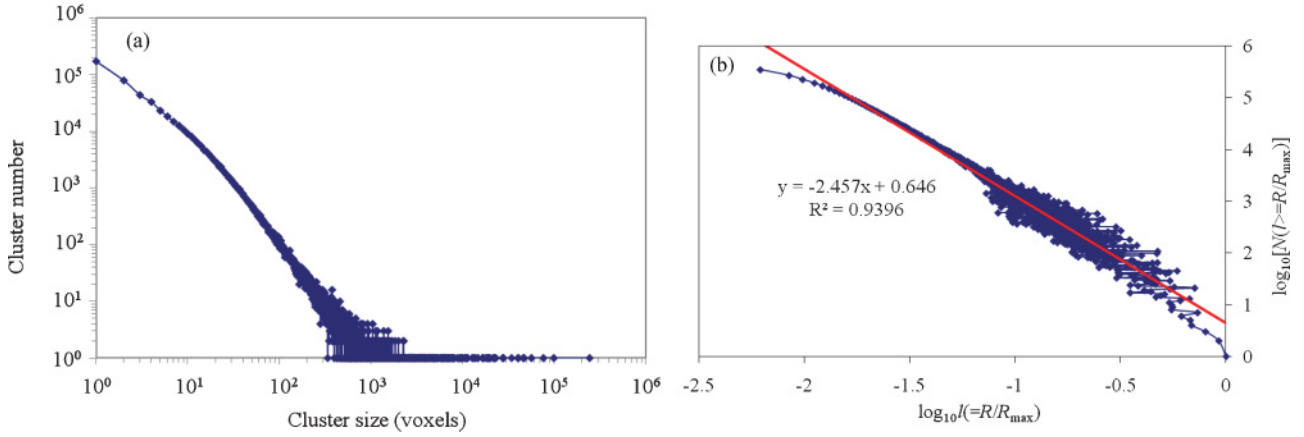

FIG. 4. (Color online) Mylonite subsample from the perimeter of the shear zone: (a) cluster size in voxels and cluster number counts exhibit two linear segments for cluster sizes larger than 10; a sharp transition to a horizontal slope is observed for cluster sizes larger than 1000; and (b) relative cluster size l and cluster number N giving fractal dimension according to Eq. (5).

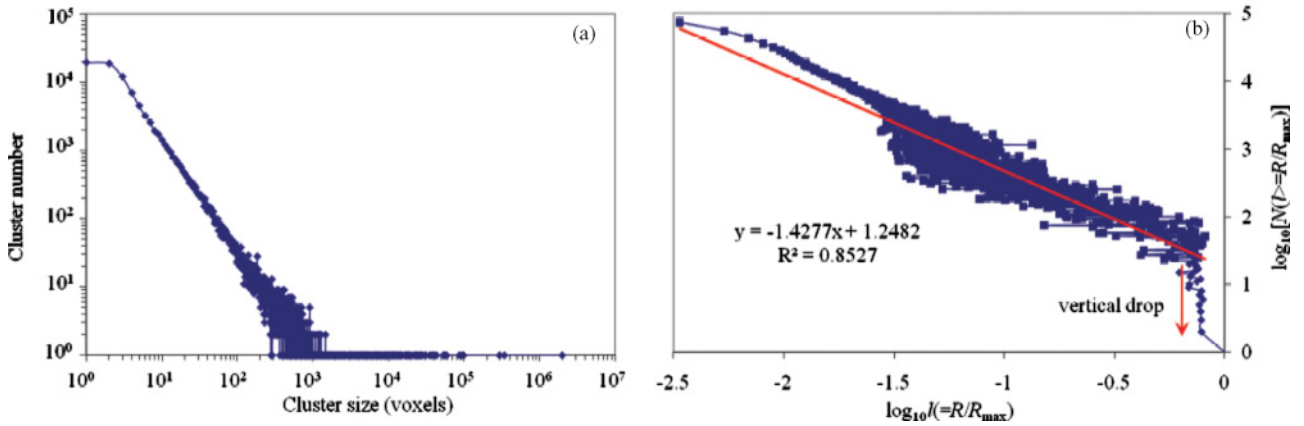

FIG. 5. (Color online) Tree branch sample: (a) cluster size in voxels and cluster number counts also show two linear segments for clusters larger than 2, and the break to a horizontal slope occurs at cluster size 1000; and (b) relative cluster size l and cluster number N giving fractal dimension according to Eq. (5); there is a vertical drop for large l in this strongly anisotropic sample.

The percolation threshold of the sample is merely 0.31%, the lowest in Table I. For this porosity, there are three percolating clusters in the derivative model. According to traditional percolation theory, percolation is achieved when the first and largest cluster is percolating and all other smaller clusters are nonpercolating. For the strongly oriented tree branch sample, this basic assumption is not valid. There are 39 clusters which are all percolating in the z direction (the growing direction) in the 400-cube volume but not in the other two directions. Owing to this important difference, the results for this strongly structured medium are quite different from those for the more isotropic examples above.

Although the distribution of the logarithm of the cluster size versus number is similar to that for the mylonite sample [see Fig. 5(a) and compare with Fig. 4(a)], the relative size of the cluster, l, versus the number N in Eq. (5) shown in Fig. 5(b) is different from that in Fig. 4(b). The most significant characteristic in Fig. 5(b) is that there is a near-vertical drop for large clusters. The reason is the strong anisotropy with multiple percolating clusters of the sample. In the tree branch, percolating clusters could be within a single conduit or several nearby conduits joined by sideways-connected cells (pit cells). According to the definition in Eq. (2), clusters with more or fewer conduits could have similar radii if conduits are not located far away from each other. The fitted line of the main part of the $\log_{10}(N)$ vs $\log_{10}(l)$ curve gives a fractal dimension of 1.427 for small clusters in Fig. 5(b). When all clusters are considered, the slope of the trend line indicates the fractal dimension of 1.486. These values are rather different from the theoretical value of 2.5 for general 3D models. Our results are consistent with previous results for wood anatomy structure, where the fractal dimension obtained by different methods was mostly in a range of $D = 1.2$–1.6 [20]. Our result is in the middle of the range and is reasonable for illustrating the characteristics of wood anatomy structure.

Stochastic analysis shows that when the subvolume size is larger than the maximum conduit diameter ($\sim$23.8 μm), the probabilities of percolation in three directions are extremely low, while the probabilities of percolation in the z direction are always much higher and have similar distributions to those shown in Fig. 3(a); see Fig. 6(a). We tried to extract the critical exponent of the correlation length from the probabilities of

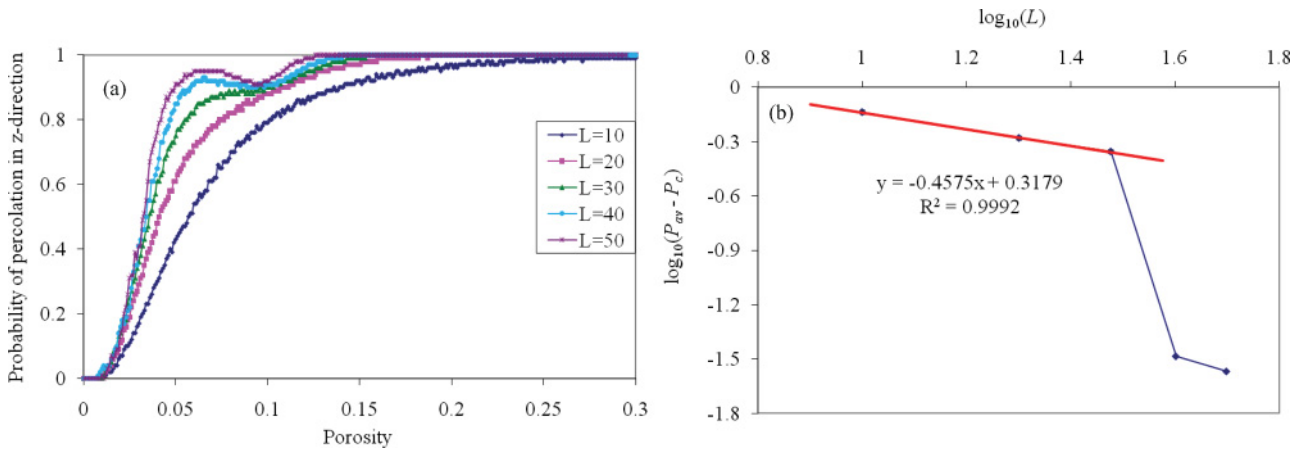

FIG. 6. (Color online) Tree branch sample. (a) Local probabilities of percolation $\lambda(p,L)$; all the starting points of $\lambda(p,L) \neq 0$ representing the percolation thresholds of finite sizes are $\leqslant$0.01. (b) The fitting of the correlation length exponent based on the results of (a) and finite-size-scaling scheme of Eq. (4); the fit of the critical exponent fails beyond a cubic size of $\log_{10}(L) = 1.6$ or $L = 40$.

percolation in the z direction of different subvolume sizes; however, the resulting curve is inconclusive [see Fig. 6(b)]. Although small subvolume sizes give an exponent of 0.4575, obviously it cannot be extrapolated to the large scale. We conclude that the finite-size-scaling scheme encounters difficulties for strongly anisotropic and heterogeneous structured media and new methods and measures need to be devised for materials of this type.

IV. SUMMARY AND RESULTS

In this paper, we have applied percolation theory to the analysis of microtomographic images and have tested the acquisition of quantities such as percolation threshold, crossover length, fractal dimension, and critical exponent of the correlation length. The ultimate goal of the analysis is to directly derive the scaling laws for upscaling of material properties from x-ray CT scan data. The approach works well on the benchmark sample, a synthetic sandstone sample. By shrinking or expanding the target phase and applying percolation analysis, we obtain a critical model and a reliable estimation of the percolation threshold. The crossover length is determined from the critical model by numerical simulations. The fractal dimension can be obtained either from the critical model or from the relative size distribution of clusters. Stochastic analysis results can be directly used to extract the critical exponent of the correlation length. The bread sample also gives similar outcomes and confirms the validity of the approach to randomly structured media.

The extrapolation of the theory to anisotropic samples gives some useful results but it fails in some aspect of the scaling relationships, particularly the derivation of the critical exponents. For the tree branch sample, multiple percolating clusters with similar sizes are encountered in one model. However, the fractal dimension is still in the range that is determined by other methods. We conclude that the finite-size-scaling scheme does not work for strongly heterogeneous and anisotropic samples, because of the failure to extract the critical exponent of the correlation length. A probable reason is that the strongly heterogeneous structure leads to additional uncertainties in the correlation length and its relevant critical exponents. For heterogeneous samples, it is possible to obtain the fractal dimension from the percolation theory analysis, but it is difficult to extract the critical exponent of the correlation length. New methods and measures need to be devised.

V. DISCUSSION

We have shown in this paper that percolation theory can be directly applied to CT scan data. The success of the application of percolation analysis to CT scan data shows that percolation theory not only is available for mathematical and experimental models but now provides a comprehensive assessment tool for any kind of tomography data set.

Percolation theory is the most direct tool for upscaling [21]. It allows the interpreter to derive scale-dependent material properties (see, e.g., Appendix C) and can be used as a robust method for identifying possible scale transitions. We propose that the same method can be used in conjunction with observations from larger-scale tomography data sets, thus providing the possibility for investigation of multifractal scale transitions. In order to make this analysis meaningful for strongly anisotropic samples, further work is still required.

The percolation threshold can be reliably obtained from deflation and inflation of the target phase for all samples when only a single CT scan is available. The estimation of the percolation threshold is an essential analysis because it significantly influences material properties [22]. The methodology developed in this paper provides the possibility to detect the relationship of material properties with the percolation threshold for any natural, structured medium. This method is necessary for most micro-CT analyses since only on the rarest occasion will more than one static image be available. A limitation of the analysis is that it only considers natural processes with isotropic changes of the structure. The degree of anisotropy of the structural changes will control the error of the method. In order to test this we have investigated micro-CT images of a melting experiment; the results will be presented elsewhere. Comparison of this melting experiment with our expansion and deflation experiment showed that the error is within the range of the natural experiment on sea ice [4]. We therefore conclude that our method is acceptable for slightly anisotropic natural processes.

The percolation thresholds listed in Table I correspond to the indicated calculated model sizes. These sizes are RVE sizes or relatively quite large sizes. We have found that these percolation thresholds are consistent with the percolation thresholds of finite sizes. Two of them, the sandstone sample and the tree branch sample, are reported in Figs. 3(a) and 6(a); the other two, the subsamples of mylonite, have been reported in Fig. 5 of Ref. [19]. We therefore conclude that the percolation thresholds detected by the deflating and inflating algorithm are valid for larger models provided that a similar structure and porosity is preserved.

The fractal dimension can be obtained reliably for all samples. This implies that the geometry can be derived accurately, thus giving a representative volume element for the geometry. This is confirmed by the convergence of the probability of porosity and percolation for all samples. Note, however, that convergence was not achieved for the probability of anisotropy of the investigated mylonite sample. We identified a shortcoming in the finite-size-scaling scheme for strongly anisotropic samples, which needs to be investigated in future studies.

The fractal dimension is a very useful quantity that can be used to assess the energetics of deformation processes for instance. In observations of highly deformed rock, geologists always find that at the center of the shear zone, the minerals are much more finely grained than at the perimeter (Fig. 1 of Ref. [18]). Our investigated mylonite sample also has a higher fractal dimension in the center than at the margin of the shear zone. According to the energy scaling law [23], the dissipated energy W after the fragmentation of a solid is proportional to the volume V to the power of $D/3$. That implies that a higher fractal dimension indicates more dissipated energy. This preliminary result demonstrates the link between the fractal dimension, energy dissipation, and deformation.

Future work will include multiphase materials. Although this paper only presented two-phase case studies (targeted pores) the approach is suitably generic to any kind of material

phase. Percolation analysis can also be applied to derive elastic percolation, electrical percolation, thermal conductivity, and many other properties. For strongly anisotropic samples we will combine the use of the probabilities of porosity, percolation, and anisotropy of microtomography with the statistical moment method. This method will allow the generation of derivative models which retain the material anisotropy. We will thus create digital samples, which represent the characteristics of the microstructure, and use these for the upscaling of properties [24].

ACKNOWLEDGMENTS

This project was funded through the Western Australian Government, the CSIRO OCE, and the Geothermal Centre of Excellence of Western Australia. We are grateful to iVEC for technical support and access to the Altix supercomputer. We greatly appreciate the contributions from the following persons: Florian Fusseis in the School of Earth and Environment, University of Western Australia who provided constructive suggestions for the paper and the micro-CT data of mylonite; Keyu Liu in CSIRO Earth Science and Resource Engineering who provided the synthetic sandstone sample images and experimental test results for permeability; Shuo Wang in CSIRO, Food Futures National Research Flagship who provided the bread sample CT images and statistical analysis results; Gerald Page in the School of Plant Biology, the University of Western Australia, who provided images of the tree branch sample; Wenlu Zhu in Maryland University who provided the images of olivine-melt samples. We also appreciate comments from Michael Glinsky, Lynn Reid, Junfang Zhang, and Ludovic Ricard of CSIRO ESRE which helped to improve the manuscript.

APPENDIX A: PERCOLATION THEORY

Percolation theory was introduced for the analysis of mathematically random models. Consider a lattice model, every site of which has the probability p to be occupied and the probability $(1 - p)$ to be unoccupied. This is the mathematical definition of a random model. In random models, every site is independent of the others. The probability p is called the concentration in percolation theory; p also stands for the volume fraction of occupied sites in the model. A typical 2D square site model is illustrated in Fig. 7, in which 60% of sites are occupied. The nearest neighbors are sites with one common line in square lattice models. A cluster is defined as a group of connected nearest neighbors which are occupied. A percolating cluster is generally the largest cluster that reaches two opposite end boundaries of the model, and in this case, the model is defined as percolating.

As the concentration p increases from 0, the average cluster size becomes larger. Only when the concentration is high enough is it possible to have a large percolating cluster. A typical probability of percolation λ versus concentration p for random models is illustrated in Fig. 8. The particular concentration at which percolation of the model first occurs is the critical percolation threshold, which is denoted as p_c. The (critical) percolation threshold is a crucial parameter, as at this point, the behavior of the model changes drastically.

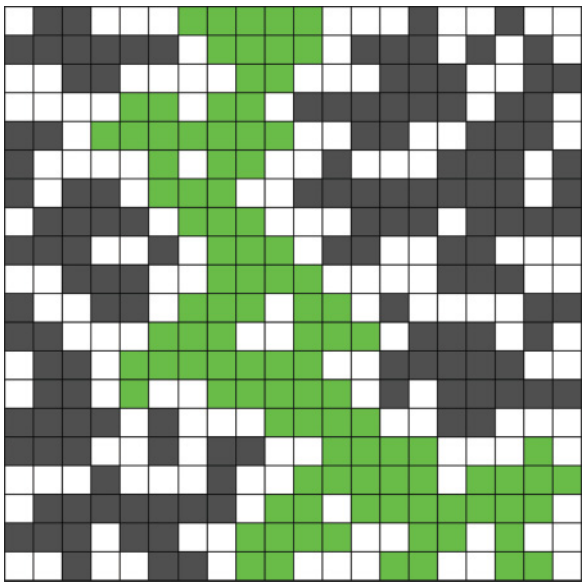

FIG. 7. (Color online) A 20×20 square lattice model with $p = 0.6$. The largest cluster (light gray, or green online) connects top and bottom boundaries; thus this mode is percolating.

For example, a porous medium turns from an impermeable into a permeable medium, a thermodynamic system has a phase transition, and a magnetic or electrical system becomes conductive. Percolation thresholds for different lattice models have been determined mathematically, e.g., for a 2D square lattice model $p_c = 0.5975$, and for a 3D simple cubic lattice model $p_c = 0.336$.

When the concentration of the model is very close to the percolation threshold p_c, the model is at the critical point and critical point phenomena occur. Percolation theory studies the percolation or connectivity of the model and the characteristics of clusters versus concentration, and focuses on the critical point phenomena and their description, including power-law divergences of some quantities described by critical exponents, the fractal dimension, universality, and scaling laws among different quantities. Many quantities and concepts are defined in percolation theory in order to describe critical point phenomena.

The most important concepts, especially used in this paper, are the correlation length, fractal dimension, and critical exponents. The correlation length is a measurement of the

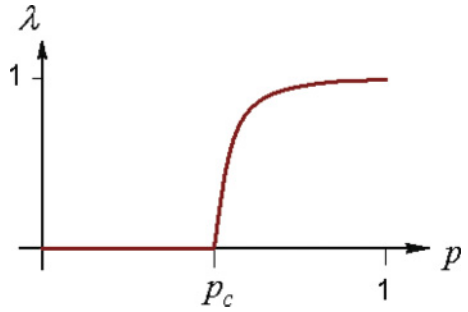

FIG. 8. (Color online) General feature of probability of percolation λ changing with concentration p. When $p < p_c$, $\lambda = 0$; when $p \geqslant p_c$, $\lambda \geqslant 0$; and $\lambda \to 1$ when $p \to 1$.

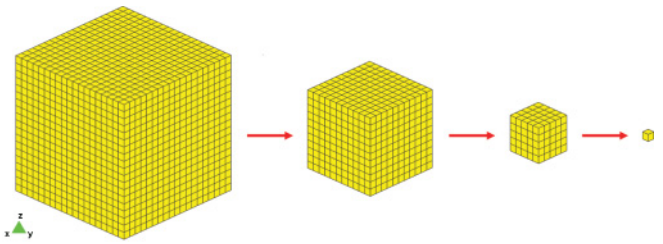

FIG. 9. (Color online) A cube becomes smaller by deflating.

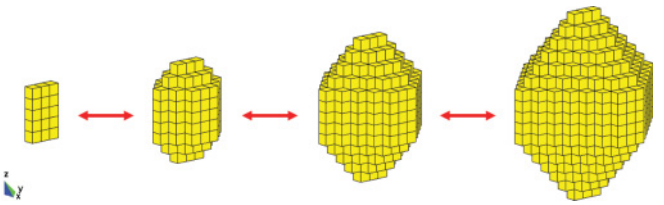

FIG. 11. (Color online) The anisotropy is changing during inflation or deflation for an anisotropic cluster.

largest "hole" in the largest cluster (holes are here understood as the areas occupied by the dark gray and white sites in Fig. 7). The fractal dimension is a statistical quantity that gives an indication of how a fragmented geometric shape occupies space at different scales. In percolation theory, there are some quantities which are divergent when the concentration p is close to the percolation threshold p_c. There exist relationships like $A \propto (p - p_c)^{-B}$, and B is called the critical exponent of A. The definitions of correlation length, fractal dimension, and critical exponent of the correlation length can be found in Ref. [3] for more in-depth reading.

APPENDIX B: THE DEFLATION AND INFLATION ALGORITHM FOR PERCOLATION THRESHOLD DETECTION

The algorithm for deflation and inflation (interchangeable with shrinking and expanding) is simple and straightforward. As mentioned in Sec. II, our analyses are built on 3D binary models. In 3D binary models, the target phase is labeled as 0 and the matrix is labeled as 1. A deflation or inflation operation is simply a modification of labels of the voxels in the model, i.e., deflation changes a label 0 to 1 for any target phase voxel that has one or more nearest neighbors belonging to the matrix, inflation changes a label 1 to 0 for any matrix voxel when it has one or more nearest neighbors belonging to the target phase. Only nearest neighbors are considered when modifying labels. This is consistent with the definition of clusters in the percolation analysis. The operations of inflation and deflation are manipulated step by step from the original model to inflation and deflation models, respectively.

The typical characteristics of deflation and inflation are briefly shown in Figs. 9–11 by three simplest structures. In Fig. 9, a cube becomes a smaller cube by deflation. In Fig. 10, a voxel becomes an octahedron by inflation. This is because the algorithm defines that only the nearest neighbors are influenced by deflation or inflation. Reversibly, an octahedron becomes a

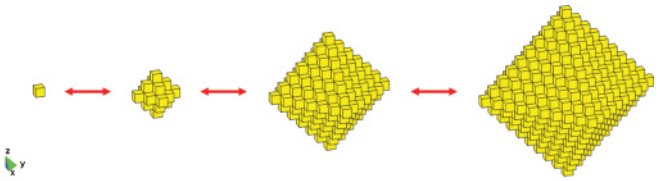

FIG. 10. (Color online) A voxel becomes an octahedron by inflating. An octahedron also turns into a voxel by deflating.

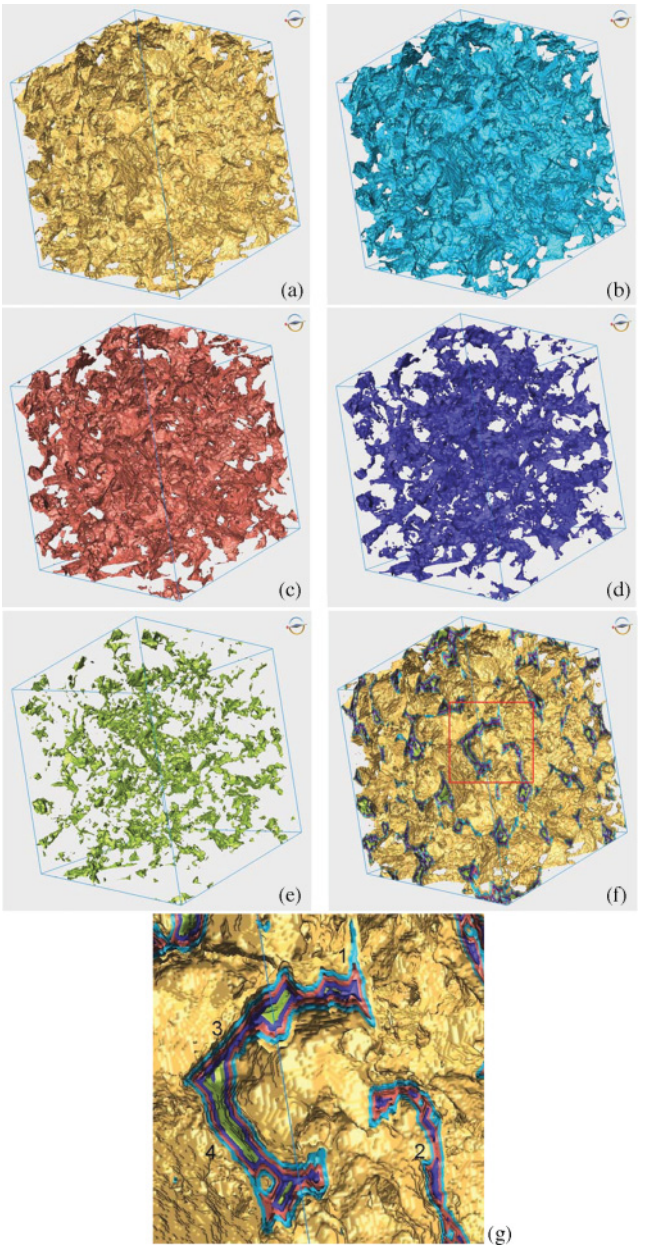

FIG. 12. (Color online) Evolution of the isosurface of the sandstone sample in a 1 mm^3 volume while shrinking the pore structure. (a) The original model; (b)–(e) after 2,4,6,8 steps of deflation, respectively; (f) combination showing original and derivative models; (g) magnified image of central part of (f); numbers 1 to 4 label the gradually sealed pores.

voxel by deflation. In Fig. 11, the anisotropy is changing while deflation or inflation occurs for an anisotropic cluster. The isotropy index (as defined and calculated in [9]) is increasing from left to right from 0 to 0.35, 0.57, and 0.70 in this figure. These figures show us that the nearest-neighbor deflation or inflation operation is not always reversible and can change the shape or the anisotropy after excessive deflation or inflation operations.

However, for a complex cluster, the algorithm works well as shown in Fig. 12 for the synthetic sandstone sample. In this case the limitations mentioned above only affect the small and isolated clusters, which are immaterial for a percolation analysis. In this first stage, the deflation or inflation operation is the most feasible and economic approach to generate derivative models.

Figure 12 shows that the isosurfaces (boundaries between grains and pores) move toward the inside of the pores while shrinking, and the decrease in volume fraction is obvious. The original model and derivative models after two and four steps of deflation [Figs. 12(a)–12(c)] have good connectivity for most pores. The model after the sixth deflation shown in Fig. 12(d) is the critical model, which is percolating only in the z direction. We can see that the connectivity is weaker in Fig. 12(d) than in Figs. 12(a)–12(c). The model after the eighth deflation [Fig. 12(e)] is not percolating and most pores are separated from each other. The overlap of the original model and derivative models together, Fig. 12(f), highlights the sealing process of pores. The magnified image of the central part of Fig. 12(f) shows clearly the progression in Fig. 12(g). The numbers in the magnified image correspond to the following: (1) a position where the pore is sealed on the second deflation; (2) and (3) positions where the pore is sealed on the fourth and sixth deflations, respectively; (4) a position where the pore is still open after eight deflation operations. This figure verifies that in natural samples a series of derivative models with similar structures but different volume fractions can be generated. It also shows that the deflation process gives acceptable deformation of complicated clusters, as we expected.

APPENDIX C: AN EXAMPLE OF UPSCALING PERMEABILITY

The permeability of the synthetic sandstone sample was computed and compared with experimental data. We used two methods to compute permeability at the microscale. The first one is the estimation of permeability according to Pittman's empirical equation [25]. It gives the relationship among the pore aperture radius r (in μm), permeability K (in mD), and porosity ϕ (in %) as

$$\log_{10} r = -0.117 + 0.475 \log_{10} K - 0.099 \log_{10} \phi, \quad \text{(C1)}$$

where r represents the pore aperture when it is interconnected to form an effective pore system that controls the fluid flow. The pore aperture has an equivalent definition as the pipe diameter $r = 4\phi/s_p$, where s_p is the specific surface area. The second method for permeability computation is the PERMSOLVER [26], which uses a finite-difference method to solve Stokes flow under a given pressure difference and microstructure.

With the RVE size 1 mm^3, we estimate the permeability using Eq. (C1) to be 4228 mD, and the computational result from PERMSOLVER is 1763 mD. Two experimental tests were carried out on the scale of centimeters (around 3.8-cm-diameter cylinder). The Klinkenberg (or air) permeability is 4500 mD, and the water permeability is 2567. The empirical estimated result is very close to the air permeability and the PERMSOLVER result is relatively close to the water permeability. Since an accurate determination of permeability is difficult for both numerical computation and experimental tests [14(b)], the differences between these results are acceptable. These comparisons show that the method for detecting the scale dependence of permeability is accurate from the crossover length of 50 μm to the centimeter laboratory scale.

[1] S. Torquato, Int. J. Solids Struct. **37**, 411 (2000); S. Youssef, E. Maire, and R. Gaertner, Acta Mater. **53**, 719 (2005).

[2] A. G Hunt, Transp. Porous Media **30**, 177 (1998).

[3] D. Stauffer and A. Aharony, *Introduction to Percolation Theory* 2nd ed. (Taylor & Francis, London, 1994).

[4] D. J. Pringle, J. E. Miner, H. Eicken, and K. M. Golden, J. Geophys. Res. [Oceans] **114**, C12017 (2009).

[5] S. R. Stock, Int. Mater. Rev. **53**, 129 (2008).

[6] J. Ikeda, S. Nakano, and T. Y. Nakashima, Mineral. Mag. **64**, 945 (2000).

[7] Y. Nakashima and S. Kamiya, J. Nucl. Sci. Technol. **44**, 1233 (2007).

[8] A. Navarre-Sitchler, C. I. Steefel, L. Yang, L. Tomutsa, and S. L. Brantley, J. Geophys. Res. [Earth Surf.] **114**, F02016 (2009).

[9] J. Liu, K. Regenauer-Lieb, C. Hines, K. Liu, O. Gaede, and A. Squelch, Geochem. Geophys. Geosyst. **10**, Q05010 (2009).

[10] E. J. Garboczi, K. A. Snyder, J. F. Douglas, and M. F. Thorpe, Phys. Rev. E **52**, 819 (1995); J. P. de Dreuzy, P. Davey, and O. Bour, *ibid.* **62**, 5948 (2000).

[11] C. L. Farmer, Int. J. Numer. Meth. Fluids **40**, 63 (2002).

[12] J. Hoshen and R. Kopelman, Phys. Rev. B **14**, 3438 (1976).

[13] R. Hilfer, Phys. Rev. B **45**, 7115 (1992); Transp. Porous Media **46**, 373 (2002).

[14] C. H. Arns, M. A. Knackstedt, W. Val Pinczewski, and W. B. Lindquist, Geophys. Res. Lett. **28,** 3361 (2001); C. Manwart, U. Aaltosalmi, A. Koponen, R. Hilfer, and J. Timonen, Phys. Rev. E **66**, 016702 (2002); M. A. Knackstedt, C. H. Arns, M. Saadatfar, T. J. Senden, A. Limaye, A. Sakellariou, A. P. Sheppard, R. M. Sok, W. Schrof, and H. Steininger, Proc. R. Soc. London, Ser. A **462**, 2833 (2006).

[15] D. P. Bentz, ACI Mater. J. **105**, 297 (2008).

[16] A. Kapitulnik, A. Aharony, G. Deutscher, and D. Stauffer, J. Phys. A: Math. Gen. **16,** L269 (1983).

[17] P. Babin, G. Della Valle, R. Dendievel, N. Lassoued, and L. Salvo, J. Mater. Sci. **40**, 5867 (2005).

[18] F. Fusseis, K. Regenauer-Lieb, J. Liu, R. M. Hough, and F. De Carlo, Nature (London) **459**, 974 (2009).

[19] J. Liu, K. Regenauer-Lieb, and F. Fusseis, in *Advances in Geosciences*, edited by K. Satake (World Scientific, Singapore, 2010), Vol. 20, p. 229.
[20] P. Konas, J. Buchar, and L. Severa, Eur. J. Mech. A/Solids **28**, 545 (2009).
[21] Y. Gueguen, M. Le Ravalec, and L. Ricard, Pure Appl. Geophys. **163**, 1175 (2006).
[22] G. W. Scherer, Am. Ceram. Soc. Bull. **70**, 1059 (1991).
[23] A. Carpinteri and N. Pugno, Nat. Mater. **4**, 421 (2005).
[24] K. Regenauer-Lieb *et al.*, in *Advances in Geocomputing*, edited by H. Xing (Springer, Berlin, 2008), p. 1; C. E. Schrank, K. Regenauer-Lieb, T. Poulet, A. Karrech, J. Liu, F. Fusseis, and O. Gaede, Specialist Group in Tectonics and Structure Geology (SGTSG) Conference 2010, abstract.
[25] E. D. Pittman, AAPG Bull. **76**, 191 (1992).
[26] [ftp://ftp.nist.gov/pub/bfrl/bentz/permsolver/].